Modes, stability, and small-signal response of photonic crystal Fano lasers

Rasmussen, Thorsten Svend; Yu, Yi; Mørk, Jesper

Published in:
Optics Express

Link to article, DOI:
10.1364/OE.26.016365

Publication date:
2018

Document Version
Publisher's PDF, also known as Version of record

Research Article | Vol. 26, No. 13 | 25 Jun 2018 | OPTICS EXPRESS 16365
Optics EXPRESS

Modes, stability, and small-signal response of photonic crystal Fano lasers

THORSTEN S. RASMUSSEN,[1,*] YI YU,[1] AND JESPER MORK[1]

[1]DTU Fotonik, Department of Photonics Engineering, Technical University of Denmark, Orsteds Pl., 2800 Kgs. Lyngby, Denmark
[*]thsv@fotonik.dtu.dk

Abstract: Photonic crystal Fano lasers have recently been realised experimentally, showing useful properties such as pinned single-mode lasing and passive pulse generation. Here the fundamental properties of the modes of the Fano laser are analysed, showing how the laser functionality depends sensitively on the system configuration. Furthermore the laser stability is investigated and linked to the small-signal response, which shows additional dynamics that cannot be explained with a conventional rate equation model, including a damping of relaxation oscillations and a frequency modulation bandwidth that is only limited by the nanocavity response.

OCIS codes: (140.0140) Lasers and laser optics; (140.5960) Semiconductor lasers; (350.4238) Nanophotonics and photonic crystals.

References and links

1. D. A. B. Miller, "Device requirements for optical interconnects to silicon chips," Proc. IEEE **97**, 1166–1185 (2009).
2. O. Painter, R. K. Lee, A. Scherer, A. Yariv, J. D. O'Brien, P. D. Dapkus, and I. Kim, "Two-dimensional photonic band-gap defect mode laser," Science **284**, 1819–1821 (1999).
3. S. Matsuo, T. Sato, K. Takeda, A. Shinya, K. Nozaki, H. Taniyama, M. Notomi, K. Hasebe, and T. Kakitsuka, "Ultralow operating energy electrically driven photonic crystal lasers," IEEE J. Sel. Top. Quantum Electron. **19**, 4900311 (2013).
4. H. Jang, I. Karnadi, P. Pramudita, J.-H. Song, K. Soo Kim, and Y.-H. Lee, "Sub-microwatt threshold nanoisland lasers," Nat. Commun. **6**, 8276 (2015). Article.
5. Y. Akahane, T. Asano, B.-S. Song, and S. Noda, "High-q photonic nanocavity in a two-dimensional photonic crystal," Nature. **425**, 944–947 (2003).
6. N.-V.-Q. Tran, S. Combrié, and A. De Rossi, "Directive emission from high-q photonic crystal cavities through band folding," Phys. Rev. B **79**, 041101 (2009).
7. P. Hamel, S. Haddadi, F. Raineri, P. Monnier, G. Beaudoin, I. Sagnes, A. Levenson, and A. M. Yacomotti, "Spontaneous mirror-symmetry breaking in coupled photonic-crystal nanolasers," Nat Photon **9**, 311–315 (2015). Letter.
8. Y. Ota, M. Kakuda, K. Watanabe, S. Iwamoto, and Y. Arakawa, "Thresholdless quantum dot nanolaser," Opt. Express **25**, 19981–19994 (2017).
9. G. Crosnier, D. Sanchez, S. Bouchoule, P. Monnier, G. Beaudoin, I. Sagnes, R. Raj, and F. Raineri, "Hybrid indium phosphide-on-silicon nanolaser diode," Nat. Photonics **11,** 297 (2017).
10. Y. Yu, W. Xue, E. Semenova, K. Yvind, and J. Mork, "Demonstration of a self-pulsing photonic crystal fano laser," Nat Photon **11**, 81–84 (2017). Letter.
11. J. Mork, Y. Chen, and M. Heuck, "Photonic crystal fano laser: Terahertz modulation and ultrashort pulse generation," Phys. Rev. Lett. **113**, 163901 (2014).
12. T. S. Rasmussen, Y. Yu, and J. Mork, "Theory of self-pulsing in photonic crystal fano lasers," Laser & Photonics Rev. **11**, 1700089 (2017).
13. Y. Yu, M. Heuck, H. Hu, W. Xue, C. Peucheret, Y. Chen, L. K. Oxenlowe, K. Yvind, and J. Mork, "Fano resonance control in a photonic crystal structure and its application to ultrafast switching," Appl. Phys. Lett. **105**, 061117 (2014).
14. D. A. Bekele, Y. Yu, H. Hu, P. Guan, L. Ottaviano, M. Galili, L. K. Oxenløwe, K. Yvind, and J. Mork, "Pulse carving using nanocavity-enhanced nonlinear effects in photonic crystal fano structures," Opt. Lett. **43**, 955–958 (2018).
15. Y. Yu, Y. Chen, H. Hu, W. Xue, K. Yvind, and J. Mork, "Nonreciprocal transmission in a nonlinear photonic-crystal fano structure with broken symmetry," Laser & Photonics Rev. **9**, 241–247 (2015).
16. S. Fan, W. Suh, and J. D. Joannopoulos, "Temporal coupled-mode theory for the fano resonance in optical resonators," J. Opt. Soc. Am. A **20**, 569–572 (2003).
17. A. M. Yacomotti, S. Haddadi, and S. Barbay, "Self-pulsing nanocavity laser," Phys. Rev. A **87**, 041804 (2013).
18. C. W. Hsu, B. Zhen, A. D. Stone, J. D. Joannopoulos, and M. Soljacic, "Bound states in the continuum," Nat. Rev. Mater. **1**, 16048 (2016). Review Article.

#326636 https://doi.org/10.1364/OE.26.016365
Journal © 2018 Received 28 Mar 2018; revised 9 May 2018; accepted 24 May 2018; published 13 Jun 2018

Optics EXPRESS

19. B. Tromborg, H. Olesen, X. Pan, and S. Saito, "Transmission line description of optical feedback and injection locking for fabry-perot and dfb lasers," Quantum Electron. IEEE J. **23**, 1875–1889 (1987).
20. W. Xue, Y. Yu, L. Ottaviano, Y. Chen, E. Semenova, K. Yvind, and J. Mork, "Threshold characteristics of slow-light photonic crystal lasers," Phys. Rev. Lett. **116**, 063901 (2016).
21. L. Coldren and S. Corzine, *Diode Lasers and Photonic Integrated Circuits,* 1st ed. (Wiley, Wiley 1995).
22. T. Baba, A. Motegi, T. Iwai, N. Fukaya, Y. Watanabe, and A. Sakai, "Light propagation characteristics of straight single-line-defect waveguides in photonic crystal slabs fabricated into a silicon-on-insulator substrate," IEEE J. Quantum Electron. **38**, 743–752 (2002).
23. P. T. Kristensen, J. R. de Lasson, M. Heuck, N. Gregersen, and J. Mork, "On the theory of coupled modes in optical cavity-waveguide structures," J. Light. Technol. **35**, 4247–4259 (2017).
24. G. Looss and D. D. Joseph, *Elementary stability and bifurcation theory,* 1st ed. (Springer, 1990).
25. B. A. Daniel, D. N. Maywar, and G. P. Agrawal, "Dynamic mode theory of optical resonators undergoing refractive index changes," J. Opt. Soc. Am. B **28**, 2207–2215 (2011).
26. M. Notomi and S. Mitsugi, "Wavelength conversion via dynamic refractive index tuning of a cavity," Phys. Rev. A **73**, 051803 (2006).

1. Introduction

With the fast development of on-chip photonics and its potential in the integrated circuits of the future, there is an increasing requirement for compact, fast and energy efficient light sources [1]. Photonic crystal lasers [2] represent a potential answer for this demand, with electrically pumped lasers that can be modulated in the GHz range already realised [3,4]. In addition to this, the ability to form ultra-small optical cavities and control the output signal [5,6] has lead to demonstrations of rich dynamics in these systems [7], as well as advances towards thresholdless lasing [8] and integration onto silicon [9].

Recently the photonic crystal membrane geometry was used to realise a novel type of laser, where one laser mirror arises by means of a Fano resonance [10]. This Fano resonance is formed by interaction of the continuum of modes of a line-defect waveguide with a discrete mode of a nearby nanocavity, leading to a high reflectivity near the resonance frequency of the nanocavity, which serves to form a laser cavity (L-Cavity) if the other end of the waveguide is blocked off [11]. Figure 1(a) shows a schematic of the laser geometry with the Fano reflection indicated, as well as decay rates used for the subsequent analysis. The second output port (upper channel in Fig. 1(a)) is included to yield a large improvement of the laser efficiency [11], but is in principle not necessary for the laser system to function. It was experimentally demonstrated that if the active region extends into the nanocavity, then this Fano laser can undergo a transition into a regime of passive pulse generation, while also having unique mode selection properties [10] and potential for ultra-fast frequency modulation [11]. This self-pulsing has subsequently been analysed in detail by development of a theoretical model based on combining coupled-mode theory (CMT) and rate equations [12]. In this work it is assumed that the active region is confined only to the waveguide, as indicated in Fig. 1, which suppresses the self-pulsing. The Fano mirror has also been shown to allow for ultrafast signal processing [13], pulse carving [14], and non-reciprocal transmission [15] when combined with carrier nonlinearities, giving ample opportunities for new laser physics and new laser functionalities.

In this paper we present a multi-mode analysis of the steady-state properties of the Fano laser, as well as analyse the stability properties and small-signal response of the laser. The paper is structured as follows: In section 2 the static properties of the device are analysed, describing how the formation of the laser cavity happens as a consequence of Fano interference, with quantitative descriptions of the reflection spectrum, quality factor, threshold gain, and laser frequency. It is also shown how the laser parameters evolve under tuning of the cavity length and nanocavity resonance frequency. Section three presents a model for the temporal dynamics of the laser, which is used to analyse the modulation response and stability properties of the system by a differential analysis. It is demonstrated how the modulation response may be strongly damped by the nanocavity, but also how the previously demonstrated unusually large intrinsic frequency

Optics EXPRESS

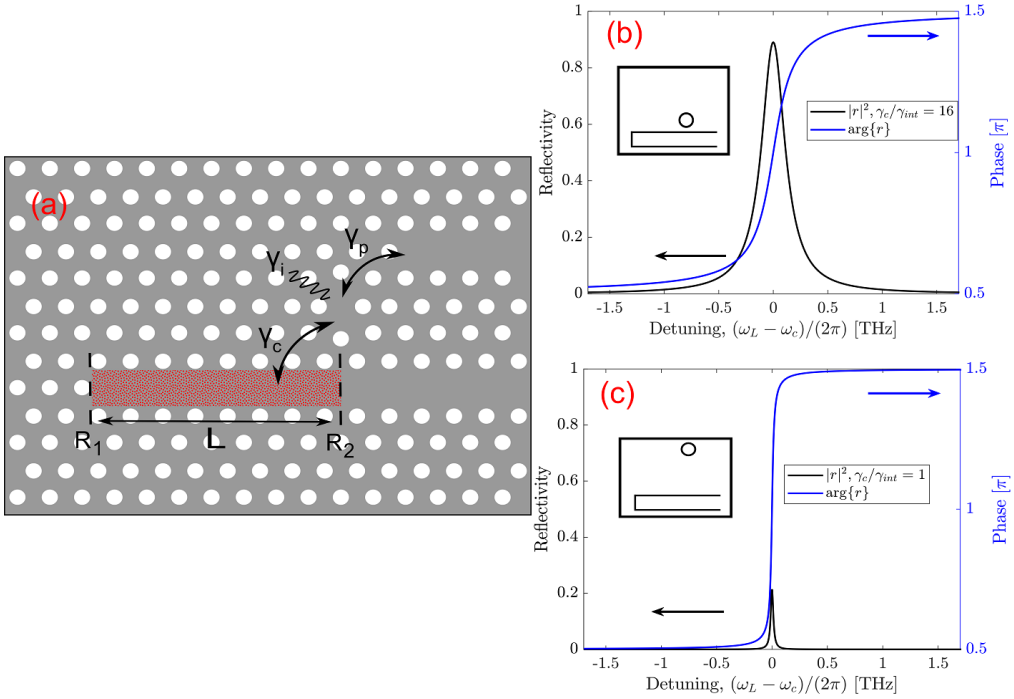

Fig. 1. (a) Schematic of the Fano laser structure. The white circles indicate air holes etched into the dielectric membrane, and the red dots indicate quantum dot active material, the arrows show possible decay channels and the dashed black lines define the effective laser mirror planes. (b) Fano mirror reflection and phase as function of frequency detuning for $\gamma_c/\gamma_{int} = 16$, where the nanocavity is in close proximity to the waveguide (see schematic inset), leading to a large peak reflectivity. (c) Fano mirror reflection and phase for the case where the nanocavity is far from the waveguide, as illustrated by the schematic inset, leading to weak coupling ($\gamma_c/\gamma_{int} = 1$) and low reflectivity.

modulation bandwidth [11] may in fact only be limited by the limitations to adiabatic wavelength conversion of the nanocavity field, promising frequency modulation many orders of magnitude faster than for conventional lasers.

2. Static cavity and laser properties

The qualitative behaviour of the waveguide-nanocavity system depends critically on the different coupling rates and particularly the relative magnitude of the waveguide coupling and the other loss sources of the nanocavity. These are quantified using the decay rates shown in Fig. 1(a), where γ_c is the coupling rate between nanocavity and waveguide, γ_i is the intrinsic loss rate of the nanocavity and γ_p is the coupling rate to the second output port, so that the total amplitude decay rate of the nanocavity field is

$$\gamma_T = \gamma_c + \gamma_{int} = \gamma_c + \gamma_i + \gamma_p \tag{1}$$

As represented here the additional decay from coupling to the third port makes no qualitative difference for the laser operation and analysis, it only serves to improve the differential quantum efficiency, so that γ_i and γ_p can be combined into γ_{int} for the subsequent analysis. The Fano resonance phenomenon can be described with conventional coupled-mode theory (CMT), which

Optics EXPRESS

yields the reflection coefficient as function of frequency detuning [11, 16]

$$r_2(\omega_c, \omega_L) = \frac{i\gamma_c}{i(\omega_c - \omega_L) + \gamma_T} \tag{2}$$

where the detuning is the absolute difference between the nanocavity resonance frequency, ω_c, and the frequency of the incoming field, ω_L. The peak reflectivity at zero detuning is

$$|r_{\max}|^2 = |r_2(\omega_L, \omega_L)|^2 = \frac{\gamma_c^2}{\gamma_T^2} = \frac{Q_T^2}{Q_c^2} = \left(1 - \frac{Q}{Q_{int}}\right)^2 \tag{3}$$

where the quality factors were introduced from the conventional definition $Q_x = \omega/(2\gamma_x)$. In the extreme case where the nanocavity is far from the waveguide (which corresponds to $\gamma_c \ll \gamma_{int}$) there is no notable energy exchange and the behaviour of the cavity and waveguide are characterised by their separate properties. As the coupling rate increases, the system morphs into a joint cavity-waveguide system, which is no longer well-described by the individual properties of the waveguide and nanocavity. Here one might intuitively think that in this high-coupling limit the system approaches two coupled cavities, as studied in e.g. [17], but this is *not* the case. Instead the system is characterised by strong coupling between waveguide and nanocavity, with the laser cavity (L-cavity) only being realised by their interaction. This is fundamentally different from the coupled cavity example, because the two coupled cavities preserve their qualitative properties independent of the coupling rate between them. This qualitative evolution of the system is illustrated in Figs. 1(b) and 1(c), which show the Fano reflection coefficient for an incoming field in the waveguide travelling towards the nanocavity. Here the insets schematically illustrate the increase in reflectivity as the nanocavity is moved closer to the waveguide. As the reflection approaches unity in the absence of internal losses in the nanocavity, the system approaches a bound mode in the continuum of the Fabry-Perot BIC type [18]. With a blockade of the left end of the waveguide serving as a highly efficient mirror, the quality factor of the laser cavity is governed by the Fano mirror reflection, as well as the Fabry-Perot (FP) resonance condition. From the Fano reflection coefficient one can calculate the steady-state properties of the laser using a transmission line approach [12, 19]. It is assumed here that the resonance of the nanocavity is sufficiently displaced from the slow-light region of the photonic crystal waveguide so that slow-light effects can be neglected, i.e. a standard value is used for the group index. If slow-light effects are important the effective length of the L-cavity is increased, as found for conventional line-defect cavities [20]. The oscillation condition then becomes

$$r_1(\omega_L) r_2(\omega_c, \omega_L) \exp\left(2iL\left[\frac{\omega_L}{c} n(\omega_L, N) - \frac{i}{2}(\Gamma g(\omega_L, N) - \alpha_i)\right]\right) = 1 \tag{4}$$

where $r_1(\omega_L)$ is the left-mirror reflection coefficient, L is the length of the laser cavity, $n(\omega_L, N)$ is the refractive index, Γ is the field confinement factor, $g(\omega_L, N)$ is the material gain, α_i is the internal loss factor and N is the carrier density. In this analysis the refractive index and gain variations are described using linear expansions

$$g(\omega, N) \simeq g_N(N - N_0) \tag{5}$$

$$\frac{\omega}{c} n(\omega, N) \simeq \frac{\omega_r}{c} n(\omega_r, N_r) + \frac{\omega - \omega_r}{c} n_g - \frac{\Gamma\alpha}{2} g_N(N - N_r) \tag{6}$$

where g_N is the differential gain, N_0 is the transparency carrier density, c is the speed of light, n_g is the group index, α is the linewidth enhancement factor, and subscript r represents a suitable expansion point. Additionally the gain, internal loss and left-mirror are assumed frequency independent over the range of interest. This assumption is justified by the narrow bandwidth of

Optics EXPRESS

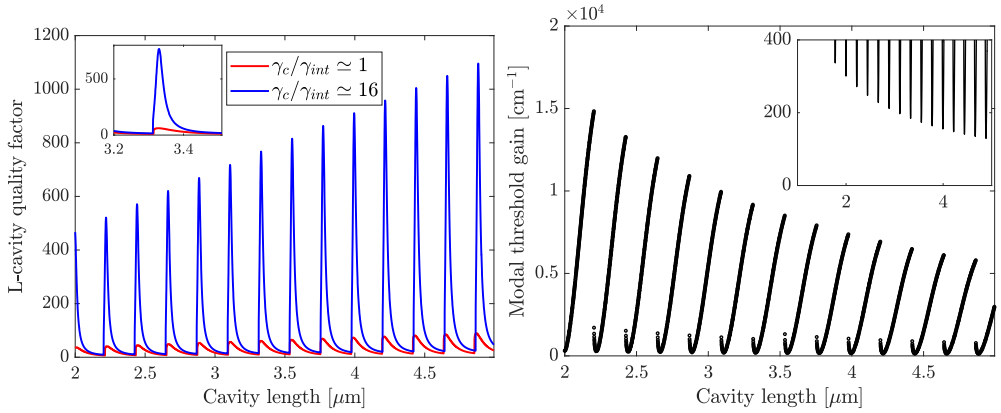

(a) (b)

Fig. 2. (a) Dependence of cavity quality factor on length of laser cavity for the two cases of Fig. 1, showing how the Q factor depends sensitively on the length. This is because a longitudinal mode must align with the nanocavity resonance in order to obtain a large Fano reflection coefficient. Inset shows a zoom in for a specific mode. (b) Modal threshold gain as function of laser cavity length for the two cases of Fig. 1. Inset shows a zoom in near the gain minima, showing how the minimum threshold gain decreases with increasing length, due to the smaller distributed mirror losses.

the Fano mirror (see Fig. 1), which is much smaller than the frequency variation range of these parameters. By separation into real and imaginary parts, the oscillation condition reduces to a highly dispersive version of the conventional laser gain and phase conditions [21] due to the strong frequency dependence of the Fano mirror, which are coupled due to the carrier dependence of the refractive index, as quantified by the linewidth enhancement factor, α. By numerical solution of the oscillation condition one can compute the threshold gain and laser wavelength as functions of the cavity length and nanocavity resonance frequency, as well as the L-cavity Q factor, which can be calculated from the threshold gain as

$$Q = \omega_L \tau_p = \frac{\omega_L}{\Gamma v_g g_{th}} \tag{7}$$

where τ_p is the photon lifetime, $v_g = c/n_g$ is the group velocity and g_{th} is the threshold gain. Figure 2(a) shows the calculated L-cavity Q factor and Fig. 2(b) shows the corresponding modal threshold gain, both as function of the L-cavity length. It is clear that the cavity only has a high quality factor, and thus low gain, for certain values of the cavity length. These are the cavity lengths where the wavelength of a resonant mode in the formed Fabry-Perot cavity aligns with the resonance frequency of the nanocavity to yield a large Fano reflection coefficient. Thus, the spacing between each minimum in the threshold gain is given by half the material wavelength corresponding to the nanocavity resonance frequency, i.e. $\Delta L = \lambda_r/(2n_r)$, except for a small correction of around 0.01% from the alpha-induced phase that stems from the change in threshold gain with length. Additionally one can see an approximately linear increase of the Q-factor with cavity length, and corresponding $1/L$ decrease of the threshold gain, which stems from decrease of the mirror losses as the length increases, as the minimum threshold gain depends approximately on $1/L$ [21]:

$$\Gamma g_{th} = \alpha_i + \frac{1}{2L} \ln\left(\frac{1}{R_1 R_2(\omega_L, \omega_c)}\right) \tag{8}$$

Optics EXPRESS

where R_1, R_2 are the mirror intensity reflectivities. Due to the short cavity lengths, the distributed mirror loss dominates over the internal loss, leading to the $1/L$ shape. By expanding Eq. (4) to second order around a reference length solution, for which the laser oscillates at the peak reflectivity, i.e. $\omega_L = \omega_c$, corresponding to a gain minimum in Fig. 2(b), one can characterise the length dependence by calculating the length change that leads to a doubling of the threshold gain, which is

$$\left(\frac{\Delta L_{\max}}{\lambda}\right)^2 = \frac{1}{16\pi^2 n^2}\left[\ln\left(\frac{1}{R_1 R_2}\right) + 2\alpha_i L\right] \tag{9}$$

For $n \approx 3.5$ and $R_1 R_2 \approx 0.9$ one finds $\Delta L_{\max}/\lambda \simeq 0.02$, suggesting that the gain changes strongly on scales of just a few tens of nanometres. This expansion of course predicts a symmetric detuning response to length tuning, but closer inspection of the threshold gain variation in Fig. 2(b) shows that there is an asymmetry in the detuning response, so that the threshold gain rises more strongly in one tuning direction. This effect stems from the gain-phase coupling signified by $\alpha \neq 0$, which in combination with the asymmetric phase variation of the Fano mirror leads to an asymmetric length tuning response [12]. This scales with the magnitude of α (vanishes for $\alpha = 0$), as well as ΔL^3, and as such is not captured by the approximation in (9). Interestingly (9) also predicts that the length tuning properties near the minima are independent of the mirror bandwidth, which seems somewhat counter-intuitive. In order to uphold the phase condition under length tuning the laser must change its frequency from the resonance, and while the phase change obtained by this frequency shift scales with $1/Q^2$, the corresponding threshold gain change scales as Q^2, because of the frequency dependence of the reflectivity, which leads to the factors cancelling. This means that the fabrication tolerance cannot simply be increased by changing the mirror bandwidth.

Figure 3(a) shows the calculated modal threshold gain of the laser as a function of the nanocavity resonance frequency shift, $\Delta\omega = \omega_c - \omega_r$, where ω_c is the nanocavity resonance frequency and ω_r represents a reference resonance frequency for which the laser frequency exactly matches the nanocavity resonance for the chosen cavity length. Here one observes that inclusion of multiple longitudinal modes (red curve) makes a key difference when the resonance is tuned by a few linewidths, where a longitudinal mode jump occurs, with the behaviour being qualitatively different when only including a single mode (blue curve). The same asymmetric tuning response around the gain minima as for the length tuning case is also evident, which is because the phase

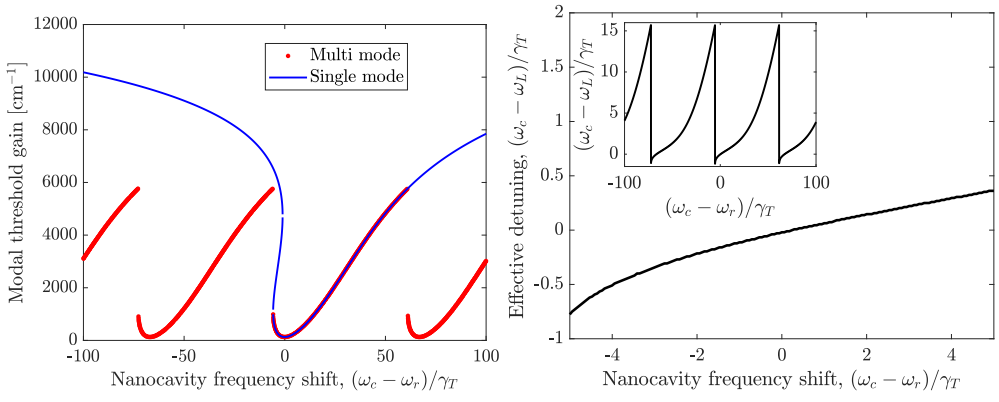

(a) (b)

Fig. 3. (a) Modal threshold gain as function of nanocavity resonance frequency shift, displaying α-induced asymmetry and periodicity. (b) Effective detuning $(\omega_c - \omega_L)$ as function of nanocavity resonance shift near zero detuning, showcasing the linear regime of Eq. (10) near each gain minimum. Inset shows the global behaviour, which is periodic.

Optics EXPRESS

condition is influenced by tuning in a similar way. However, it is worth noting how the gain curve is completely periodic when frequency tuning, because the Fano reflection only depends upon the difference between the laser frequency and nanocavity resonance frequency and not the absolute frequency, unlike the length tuning case which includes the $1/L$ dependence. Figure 3(b) shows the effective detuning, $\omega_c - \omega_L$, as a function of the nanocavity resonance shift. This curve displays the same periodicity as the gain curve, which underlines the coupling of phase and amplitude conditions. Near each gain minimum there is a regime of nearly linear variation, where the laser frequency approximately tracks the nanocavity resonance frequency. This linear regime is well-described by an expansion similar to that in (9). Making a similar analysis but this time fixing the length and allowing for a variation of the nanocavity resonance frequency by an amount $\Delta\omega_c$ from the same reference point, one finds for the corresponding change in laser frequency

$$\Delta\omega_L = \left(\frac{1}{1+\tau_{in}\gamma_T}\right)\Delta\omega_c \tag{10}$$

where $\tau_{in} = 2Ln_g/c$ is the L-cavity round-trip time. This demonstrates how the laser frequency approximately tracks the resonance frequency in the case where the round-trip time is much smaller than the field storage time in the nanocavity, i.e. $\tau_{in}\gamma_T \ll 1$, as can be seen in Fig. 3(b), where $\tau_{in}\gamma_T = 0.09$. The physical interpretation of this is that as the nanocavity resonance is changed both the waveguide propagation phase and mirror phase change, and serve to compensate each other, which reduces the effective frequency shift of the laser compared to the nanocavity resonance. The simplest example to explain this is the case of the isolated nanocavity, where the laser frequency would follow an increase, say, in the nanocavity resonance exactly to uphold the phase condition. Since the phase accumulated during propagation in the waveguide increases with frequency, however, the net phase change of the cavity has to be negative, leading to oscillation at a frequency just below the reflection peak and the appearance of the sub-unity coefficient in (10). As the waveguide phase scales directly with τ_{in} and the mirror phase change is proportional to its first derivative, which is $\mathrm{d}\phi/\mathrm{d}\omega = 1/\gamma_T$ at resonance, the product of these measures how well the round-trip phase change compensates the mirror phase change. This behaviour reflects the previously discussed bandwidth independence of (9).

The parameters used throughout, unless otherwise specified, are $Q_c = 780, Q_p = 15000, Q_v = 100000, \lambda_r = 1.554\mu\mathrm{m}, r_1 = -1, \alpha_i = 10\mathrm{cm}^{-1}, n = n_g = 3.5, \alpha = 1, \Gamma = 0.01, v_g = c/n_g, g_N = 5\times10^{-16}\mathrm{m}^{-2}, N_0 = 5\times10^{21}\mathrm{m}^{-3}, L = 4.88\mu\mathrm{m}, A = 0.20\mu\mathrm{m}^2$, where A is the cross-sectional area of the laser cavity. These are chosen based on conventional laser parameters and FDTD simulations to reflect the fabricated devices of [10]. As for the design of the PhC structure, the material, hole radius, slab thickness and lattice constant should be chosen such that guided modes of the line-defect waveguide coincide with the nanocavity resonance at the wavelength of choice. An example of this is the fabricated devices in [10], which consisted of a 250 nm thick InP membrane with a lattice constant of 455 nm and a hole radius of 110 nm. It should also be noted that the laser mode is TE-like, due to the bandgap properties of the line-defect waveguide [22].

3. Laser dynamics

A dynamical model for the laser may be derived by combining the transmission line description with coupled-mode theory and conventional rate equations. The framework and derivations of this model are given in [10, 12], so only a brief description is presented here. By Taylor expansion of the oscillation condition, one can derive an evolution equation for the right-propagating complex field amplitude, $A^+(t)$, in the laser cavity. This is combined with a CMT description of the nanocavity field, $A_c(t)$ [16, 23], and a conventional rate equation describing the dynamics of the

Optics EXPRESS

free carrier density, $N(t)$ [21]:

$$\frac{\mathrm{d}A^+(t)}{\mathrm{d}t} = \frac{1}{2}(1-i\alpha)\left(\Gamma v_g g_N(N-N_0) - \frac{1}{\tau_p}\right)A^+(t) + \gamma_L\left[\frac{\sqrt{\gamma_c}A_c(t)}{r_2(\omega_L,\omega_c)} - A^+(t)\right] \tag{11}$$

$$\frac{\mathrm{d}A_c(t)}{\mathrm{d}t} = (-i\Delta\omega - \gamma_T)\,A_c(t) + i\sqrt{\gamma_c}A^+(t) \tag{12}$$

$$\frac{\mathrm{d}N(t)}{\mathrm{d}t} = \frac{\eta_p J}{eV_{LC}} - R(N) - \Gamma v_g g_N(N(t)-N_0)\sigma(\omega_L,\omega_C)\frac{|A^+(t)|^2}{V_{LC}} \tag{13}$$

Here $\gamma_L = 1/\tau_{in}$ is the inverse of the cavity roundtrip time, and $r_2(\omega_L,\omega_c)$ and τ_p are the values of the complex Fano reflection coefficient and photon lifetime at the expansion point. Furthermore, $\Delta\omega = \omega_c - \omega_L + \Delta\omega_{NL}$ where $\Delta\omega_{NL}$ can represent non-linear frequency shifting effects, but these are neglected here. In Eq. (13) $\eta_p J/(eV_{LC})$ represents the effective pump rate, with J being the drive current, e being the elementary charge, $V_{LC} = LA$ is the volume of the laser cavity where current is being injected, and η_p the pump efficiency (set to unity throughout), while $R(N)$ is the carrier recombination rate, for which the lifetime approximation is used, i.e. $R(N) \simeq N/\tau_s$, where τ_s is an effective carrier lifetime. Finally $\sigma(\omega_L) = \frac{2\epsilon_0 n n_g}{\hbar\omega_L}\left\{\frac{1}{\Gamma g_{th}-\alpha_i}\frac{(|r_1|+|r_2(\omega_L)|)(1-|r_1||r_2(\omega_L)|)}{|r_1|} + \frac{c}{\omega_s n}\frac{|r_1|}{|r_2|}\mathrm{Im}(r_2)\right\}$ is a parameter relating the total photon number in the cavity, $I(t)$, and the field strength through $I(t) = \sigma|A^+(t)|^2$ [19]. It should be noted that for a given choice of L and ω_c, one must use the corresponding ω_L, r_2, σ_s and τ_p computed from the oscillation condition as parameters in the ODE system. With this formulation the output power in the through-port (TP) and cross-port (CP) are [10]

$$P_t(t) = 2\epsilon_0 nc\left|\sqrt{\gamma_c}A_c(t) - iA^+(t)\right|^2 \tag{14}$$

$$P_x(t) = 2\epsilon_0 nc\gamma_p|A_c(t)|^2 \tag{15}$$

3.1. Stability analysis and small-signal response

Separating the dynamical equations for $A^+(t)$ and $A_c(t)$ into amplitude ($|A|$) and phase ($\arg\{A\}$) components and performing a small-signal analysis yields the following system of differential equations describing the small-signal response:

$$\dot{\vec{x}}(t) = \mathbf{A}\vec{x}(t) + \vec{F} \qquad \vec{x} = [\delta|A^+|, \delta|A_c|, \delta\phi^+, \delta\phi_c, \delta N]^T \tag{16}$$

Here δ indicates a differential change, $\mathbf{A}$ is the system matrix of small-signal coefficients, the dot represents the time derivative, and $\vec{F}$ is a forcing function representing e.g. external modulation or quantum noise. The solutions to this system evolve from the expansion point as $\mathbf{x}(t) = \mathbf{v}\exp(\lambda t)$ where $\mathbf{v}$ is an eigenvector of $\mathbf{A}$ and λ is the corresponding eigenvalue [24]. The general structure of the eigenvalue spectrum is that of two sets of complex conjugate eigenvalues and a fifth eigenvalue which is trivially zero, because the system evolution only depends upon the phase difference between the nanocavity and waveguide fields and not the absolute phases, meaning that one phase can be chosen arbitrarily. The real part of all eigenvalues is negative over the entire phase space, signifying that the continuous-wave laser operation is stable towards perturbations. This is in sharp contrast to the case where the active material extends to the nanocavity, which results in a well-defined parameter region in which the laser transitions into self-pulsing [10] due to relaxation oscillations becoming un-damped, as signified by a pair of complex eigenvalues crossing the imaginary axis and gaining positive real parts [12].

The presence of two sets of complex conjugate eigenvalue pairs signifies two system resonance frequencies, with one corresponding to the conventional relaxation oscillations of semiconductor lasers. The other resonance frequency reflects a beating between nanocavity and laser fields with a frequency given by the effective detuning (Fig. 3(b)). This resonance is heavily overdamped and

Optics EXPRESS

does not contribute notably to the laser properties, but it is noted that the eigenvalue imaginary part exactly matches the effective detuning.

Assuming a harmonic time dependence of the variables as a response to a harmonic modulation of e.g. the pump rate, one can calculate the intensity and frequency modulation response using Cramer's rule by choosing a suitable form of the forcing function in (16). Because of the dynamical dependence upon the nanocavity resonance frequency, the laser can also be modulated through this path, adding additional functionality to the system. The conventional intensity modulation (IM) response (modulating the current) can be compared with the response of the equivalent Fabry-Perot semiconductor laser with mirror reflectivities r_1, r_2 (peak value, zero detuning), as is done in Fig. 4(a), which shows the calculated 3 dB bandwidths for Fano lasers with three different combinations of intrinsic and coupling quality factors yielding the same reflectivity. Here the forcing function is $\vec{F} = J_x\eta_p/(eV_{LC})[0,0,0,0,1]^T$, which represents a harmonic modulation of the drive current with amplitude J_x. With the same reflectivity the lasers are indistinguishable in the conventional rate equation model, leading to a prediction of identical modulation response. This is not the case, however, as is seen from the large variation in 3 dB bandwidth. Calculations show that the conventional semiconductor model and the model used here result in identical photon densities over the parameter space, so that is not the cause of this disparity. It is evident that the higher the total quality factor of the nanocavity, the stronger the damping of the response, leading to a significant decrease in both the absolute value of the bandwidth and the current slope. This is because the storage time in the nanocavity becomes comparable to the relaxation oscillation time constant, leading to an additional slow-down of the laser response. As the nanocavity Q is then reduced (while maintaining the same reflectivity) the bandwidth increases and eventually approaches the corresponding FP result, as the nanocavity storage time becomes negligibly small compared to the relaxation oscillation time constant. This is in agreement with the dynamical model, which converges to the conventional rate equation model if the nanocavity field can be adiabatically eliminated, i.e. $\gamma_T \gg \gamma_c, \gamma_L, 1/\tau_s$.

An alternative, more general, measure of comparison lies in the eigenvalues of the system matrix **A**. The set of eigenvalues corresponding to the relaxation resonance from the small signal analysis corresponds directly to the poles of the IM transfer function for the conventional FP

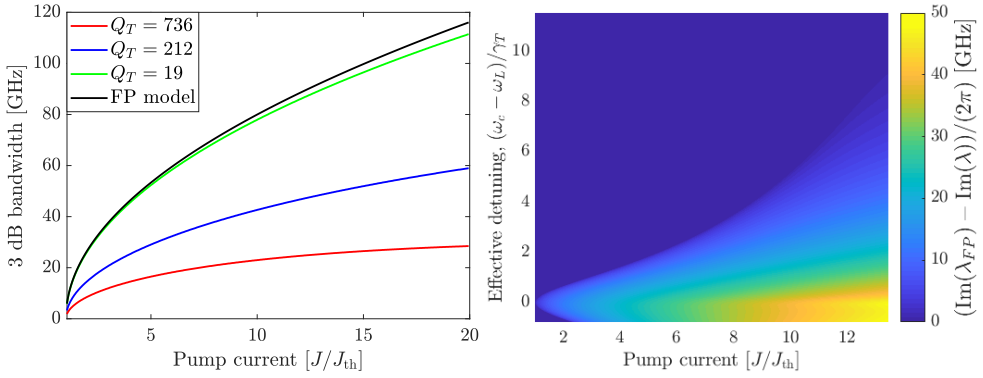

(a) (b)

Fig. 4. (a) 3 dB bandwidth as function of bias current for zero detuning. Here the FP curve is identical for all 3 cases, and the system converges towards the FP curve as the nanocavity Q decreases towards zero. (b) Absolute difference in relaxation resonance frequency between Fano laser and equivalent FP laser as function of effective detuning and pump current showing significant differences. Here $Q_T = 736$.

Optics EXPRESS

lasers, which are [21]

$$\lambda_{FP} = -\frac{\gamma}{2} \pm \sqrt{\frac{\gamma^2}{4} - \omega_{rel}^2} \tag{17}$$

with the damping coefficient γ and relaxation oscillation frequency in absence of gain compression and spontaneous emission noise being given by [21]

$$\gamma = \frac{1}{\tau_s} + v_g g_N N_p \qquad \omega_{rel}^2 = \frac{v_g g_N N_p}{\tau_p} \tag{18}$$

where N_p is the photon density, which can be calculated as $N_p = \Gamma\sigma_s|A^+|^2/V_{LC}$. We note that $\gamma \ll \omega_{rel}$ in the regimes analysed here, as is also typically the case for conventional semiconductor lasers. Figure 4(b) shows the difference between the imaginary parts of the FP eigenvalue and the corresponding eigenvalue pair from the small-signal analysis for the case where $Q_T = 736$. Here the large difference between the FP result and the small-signal analysis reflects the behaviour of Fig. 4(a), with the equivalent FP laser relaxation oscillation frequency being notably larger. This difference is also attributed to additional damping introduced by the nanocavity storage time, which, for high Q values leads to a notable slow-down of the response. One notes that the difference increases with power, similar to the tendency in Fig. 4(a). Furthermore, there is a decrease in the difference with the nanocavity resonance shift, which stems from a decrease in the intracavity photon number due to the decrease in reflectivity, leading to a smaller relaxation oscillation frequency in both cases, and thus a smaller absolute difference. These considerations demonstrate how the introduction of the Fano resonant mirror leads to additional dynamic effects that are not captured by the equivalent rate equation model.

For the case of modulating the laser through the nanocavity resonance frequency, the corresponding forcing function is $\vec{F} = \epsilon\gamma_T[0, 0, 0, 1, 0]^T$ in (16). As the mirror phase and reflectivity both depend on the nanocavity resonance cf. Fig. 1, this type of modulation generally leads to coupled modulation of the phase and amplitude simultaneously, leading to a second type of amplitude-phase coupling in addition to the effect of the linewidth enhancement factor. As such, there is both an intensity response and a frequency response associated with this modulation,

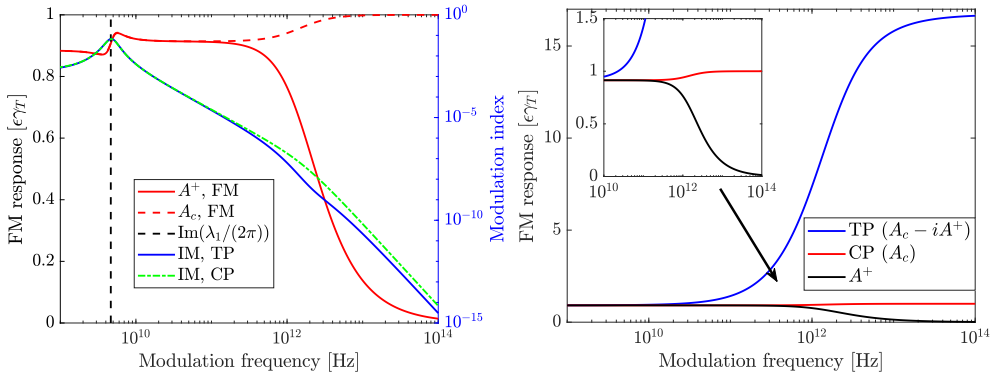

Fig. 5. (a) FM response (left axis) for A^+ (full red) and A_c (dashed red) for $3\gamma_T$ detuning of ω_c (effective detuning is $0.22\gamma_T$), with the accompanying IM response (right axis) as quantified by the modulation index in the through-port (TP, blue) and cross-port (CP, dashed green). The dashed black line indicates the relaxation resonance predicted by the eigenvalue analysis. (b) FM response at zero detuning for the throughport (TP, blue), cross-port (CP, red) and A^+. Here the resonance vanishes, because the reflectivity slope is zero.

Optics EXPRESS

except in the case where one operates exactly at zero detuning, for which the first derivative of the reflectivity is zero, meaning that in the small-signal approach there is no intensity modulation. This can be observed in Fig. 5(a), which shows the frequency and intensity response for a harmonic modulation of the nanocavity resonance frequency with the resonance offset initially by $3\gamma_T$ leading to an effective detuning of $0.22\gamma_T$. Here one can see how the intensity response (blue and dashed green lines for the through- and cross-ports respectively, right axis) resembles that of a conventional semiconductor laser with a resonance at the relaxation oscillation frequency predicted by the eigenvalue analysis (dashed grey line) and then a strong damping as the modulation frequency becomes too fast for the carrier dynamics to follow. The intensity response is quantified using the modulation index, which is defined as the maximum power fluctuation divided by the steady-state power.

The full and dashed red lines in Fig. 5(a) show the corresponding frequency response (left axis) for A^+ (full) and A_c (dashed) respectively. The frequency response is quantified as the maximum frequency variation normalised to the maximum variation of the nanocavity resonance, which is $\epsilon\gamma_T$. For low modulation frequencies the two fields have identical responses and converge towards a constant value of $\Delta\omega_L/\Delta\omega_c = 0.9142$, which is exactly the value predicted by (10). This behaviour reflects the slope of the steady-state frequency change, as shown in Fig. 3(b), which governs the response when the modulation is slower than all characteristic time scales of the system. One sees also that the FM response has a resonance at the same frequency as the IM response, but with a different shape. This resonance in the FM response arises from the phase-amplitude coupling mediated by the Fano mirror, which results in the frequency variation being proportional to the negative of the derivative of the amplitude variation. Thus, the resonance of the intensity response carries over into the FM response, but the shape is that of the negative derivative of the IM response, as can be seen in Fig. 5(a). The resonance in the FM response is also present for $\alpha = 0$, when operating at non-zero detuning, which underlines how the amplitude and phase couple through the mirror. Additionally it should be mentioned that non-linearities also lead to coupling, as was observed in [11].

Beyond this resonance one observes that the response for A^+ falls off, while that of A_c rises and then settles at around 10 THz. An explanation for this difference can be found in the nature of the dynamical equations describing the time evolution: The dynamical equation for A^+ is based on an expansion of the transmission line description, for which the temporal resolution is limited to the round-trip time in the L-cavity, meaning that dynamics faster than this time scale cannot be properly resolved, which is why the response falls off. The nanocavity field, however, is described by the CMT equation, and this is valid as long as the quality factor of the cavity is high enough and does not in principle depend upon the input, meaning that the high-frequency modulation is also well-resolved. The nanocavity field then directly tracks the input modulation by means of adiabatic wavelength conversion [25], which is why the response does not decrease for large modulation frequencies.

Figure 5(b) shows a comparison of the FM response for $A^+(t)$ (black), the through-port field ($\sqrt{\gamma_c}A_c(t) - iA^+(t)$, blue) and the cross-port field ($i\sqrt{\gamma_p}A_c(t)$, red). It is clear that the cross-port tracks the nanocavity field directly, because the two fields are directly proportional. The through-port response, however, grows strongly and exceeds the input modulation for high frequencies. This appears to be a result of the steady-state (bias) amplitude of the through-port field being very small, bringing into question the validity of the small-signal analysis. However, initial calculations with a high-resolution travelling wave model with no small-signal assumptions actually agree with the small-signal result for frequencies up to ≈ 1 THz. In-depth analysis of this interesting phenomenon is beyond the scope of this work.

The key point is that these calculations suggest that the FM bandwidth of the laser appears to only be limited by the adiabatic wavelength conversion process of the nanocavity field, and as such may be many orders of magnitude larger than for conventional semiconductor lasers. This

Optics EXPRESS

is a consequence of the modulation frequency being much faster than the time scale for carrier dynamics, so that the laser field simply tracks the nanocavity field without deviation leading to an essentially pure FM signal, as can also be seen in Fig. 5(a). In support of these considerations it has been demonstrated numerically that the adiabatic wavelength conversion process can take place over just a few femtoseconds if the refractive index modulation of the nanocavity is spatially uniform [26], meaning that one can potentially achieve frequency modulation over hundreds of THz if such an index modulation can be successfully realised.

4. Conclusion and scope

In this work a steady-state analysis of the fundamental properties of the modes of the photonic crystal Fano laser was presented. It was demonstrated how the laser threshold gain depends strongly on the nanocavity resonance frequency and the cavity length, showing the static tuning properties of the laser. It was also shown how inclusion of the Fano resonant mirror leads to modifications to the dynamical characteristics of the laser, and that these modifications are not captured by a conventional rate equation model. In particular, the storage time of the nanocavity leads to additional damping of the modulation response and it was shown how this type of mirror also leads to direct amplitude-phase coupling, even for $\alpha = 0$. Furthermore, calculations showed that the FM bandwidth of the laser may be orders of magnitude larger than that of conventional semiconductor lasers, in agreement with earlier predictions, only limited by the limits to adiabatic wavelength conversion of the nanocavity field if one can modulate the refractive index of the nanocavity directly, suggesting potential for applications in e.g. ultra-fast on-chip communication. Future work thus includes devising high-resolution temporal models for studying the ultra-fast laser dynamics, as well as practical realisations of high-speed refractive index modulations in the nanocavity.

Funding

Villum Fonden (8692)

Disclosures

The authors declare that there are no conflicts of interest related to this article.